Full title:

Iterative delivery of mRNA by MEFI

Yun Gao,[1] Huan Li,[1] Yue Xun,[1] Yu Liu,[1] Yaoyang Zhang,[1] Shuai Liu,[1] Xiaobin Fang,[1] Xiaojiao Shan,[1] Junhua Liu,[2] Qinyao Zhu,[1] Xiushan Yin,[1,3,4,*] and Luo Zhang[2*]

[1] Roc Rock Biotechnology (Suzhou) Co., Ltd. Suzhou 215000, China.

[2] Department of Computational and synthetic Biology, the Medical Innovation Research Division of Chinese PLA General Hospital, Beijing 100853, China.

[3] Biomedical Sciences College, Shandong First Medical University, Ji'nan 250117, China.

[4]Lead contact

[*]Correspondence: xiushanyin@me.com (X.Y.), marbleluo@126.com (L.Z.)

Graghical Abstract

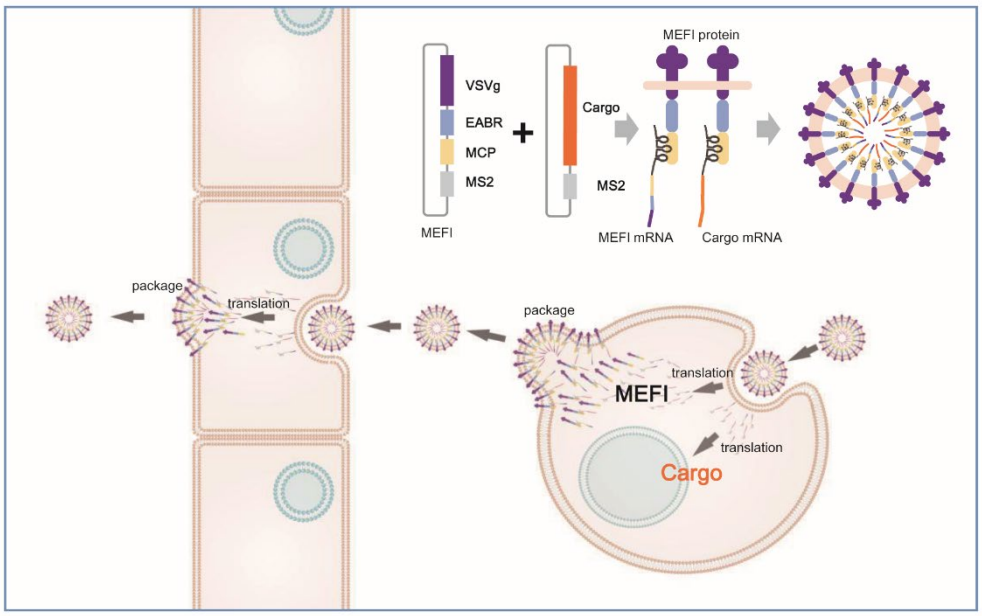

Abstract

Conventional therapeutic mRNA delivery systems are inherently single-use, limiting expression potency, duration, and penetration across biological barriers. To address this, we engineered the mRNA Exporting and Ferrying Implement (MEFI), a platform that enables iterative cell-to-cell transfer of cargo mRNA, allowing a single mRNA molecule to be utilized multiple times across various cells. MEFI encodes a fusion protein that assembles virus-like particles (VLPs) and encapsulates both itself and cargo mRNA into these VLPs, orchestrating reproduction of VLPs from targeted cells and continuous intercellular spreading. MEFI significantly amplified cargo protein expression in the transfected cell populations (~20-fold) and in organs (~500-fold in lung) from mice administered systemically. Notably, through intramuscular injection of naked plasmids, MEFI promoted robust (~20-fold) and durable (~2-month) cargo expression, interorgan mRNA transfer, and successful crossing of the blood-brain barrier. Moreover, modified MEFI demonstrated cell-type-specific targeting, mediating the elimination of antigen-expressing cells. Collectively, MEFI establishes a modular platform for enhancing mRNA delivery, leveraging the concept of iterative delivery of mRNA.

Introduction

Messenger RNA (mRNA)-based therapeutics have emerged as a transformative platform for treating diverse diseases, including infectious diseases, cancers, and genetic disorders[1-4]. Innovations in mRNA engineering and lipid nanoparticle (LNP) delivery have significantly enhanced stability and translational efficiency, exemplified by the rapid development of COVID-19 vaccines[5,6]. However, a fundamental limitation persists: current mRNA therapies operate through a "single-use" paradigm - delivered mRNA functions transiently within individual cells before degradation. This restricts protein production, hampers delivery across biological barriers (e.g., blood-brain barrier), and limits efficacy in poorly accessible tissues. To overcome these constraints, strategies enabling intercellular mRNA transfer are highly desirable.

Virus-like particles (VLPs) present a promising approach for the transfer of intercellular mRNA by encapsulating cargo during the budding process from producer cells[7-14]. Yet, conventional VLP systems require multiple viral components (e.g., gag, pol) for assembly[15-20], increasing complexity and immunogenicity[21]. While the overexpression of the vesicular stomatitis virus glycoprotein (VSVg) can lead to the release of simplified VLPs, their packaging efficiency for cargo mRNA remains low in the absence of capsid proteins[22]. Critically, no existing system achieves iterative transfer, where cargo mRNA delivered to primary cells initiates secondary production of VLPs, amplifying cargo expression across cell populations.

Here, we propose a minimalist design to enable self-propagating mRNA delivery. Many enveloped viruses recruit endosomal sorting complex required for transport (ESCRT)-associated proteins such as TSG101 and/or ALIX through capsid to conduct the budding and releasing process[23-29]. TSG101 and ALIX are also recruited by the protein CEP55 through a short amino acid sequence termed ESCRT- and ALIX-binding region (EABR) in the process of cytokinesis[30-32]. Thus, fusing the EABR to the cytoplasmic tail of a viral glycoprotein or other membrane protein directly recruits TSG101 and ALIX, bypassing the need for co-expression of other viral proteins for VLP self-assembly[33]. The aptamer MS2 and its interacting aptamer-binding protein,

MS2 coat protein (MCP), have been widely used[34-36]. VSVg mediates broad tropism and fusion via LDL receptor interaction[37,38]. By integrating these elements, we engineered a single chimeric protein, VSVg-EABR-MCP (VEM), that autonomously assembles mRNA-packaging VLPs. Furthermore, we inserted MS2 aptamers into the 3'UTR of VEM mRNA, creating a self-packaging entity termed mRNA Exporting and Ferrying Implement (MEFI). This design enables MEFI to: export both cargo mRNA and itself via VLPs; initiate VLP re-production in target cells, establishing iterative transfer cycles; serve as a modular platform capable of cell-specific delivery. Collectively, MEFI establishes a paradigm for self-propagating mRNA delivery via recursive VLP assembly and intercellular transfer.

Results

VSVg-EABR-MCP fusion protein assembles VLP that enabling MS2-tagged mRNA delivery

Traditional VLPs typically rely on capsid proteins for self-assembly and fusogens for target-cell binding and fusion. To engineer a single protein fulfilling both roles, we fused the human CEP55-derived EABR domain to the C terminus of VSVg's cytoplasmic tail via a flexible Gly-Gly-Gly-Ser linker, appending green fluorescent protein (GFP) for visualization (Figure 1A). The transient transfection of the VSVg-EABR-GFP plasmid led to the localization of GFP around the membrane in human HEK293T cells (Figure S1A). Electron microscopy images indicated that spherical, ~160-nm-diameter particles were contained in the supernatant (Figure. 1B). Subsequently, the supernatant was collected and concentrated to infect murine RAW264.7 cells. Fluorescence microscopy and flow cytometry assays indicated that the majority of the cells were GFP-positive, suggesting that the VSVg-EABR-GFP VLPs mediated effective cross-species transduction (Figure 1C and Figure S1B).

For mRNA delivery, GFP was replaced with the MS2 coat protein (MCP) to recruit MS2-tagged cargo mRNAs (Figure 1D). To define the roles of VSVg, EABR, and MCP in mRNA packaging and delivery, we generated element-deletion variants (Figure 1E). Co-transfection of mCherry-MS2 with the VSVg-EABR-MCP chimera (VEM) resulted in >2,000-fold enrichment of packaged mCherry-MS2 mRNA in supernatants of HEK293T cells (RT-qPCR), relative to controls lacking VEM. In parallel, we observed that VSVg, EABR, and MCP were all essential for mRNA packaging (Figure 1F). Subsequently, the filtered supernatant was used to infect RAW264.7 cells, and the cargo mRNA in these cells was assayed. As expected, VEM efficiently delivered mCherry mRNA into target cells. In contrast, negligible cargo mRNA was detected when either VSVg, EABR, or MCP was omitted (Figure 1G). Similar results were obtained when NLuc was used as the cargo (Figure S1C). In agreement, the expression of mCherry protein in infected cells by flow cytometry assay confirmed that all three elements are necessary for functional mRNA packaging and delivery (Figure 1H). These results

101 suggest that VSVg-EABR-MCP fusion protein assembles VLP that enabling MS2-
102 tagged mRNA package and delivery.

103 **MEFI orchestrates cargo mRNA transfer from cell to cell iteratively in vitro**

104 Current mRNA delivery systems confine translation to a single cell before degradation.
105 We posited that the iterative production of VLPs packaging cargo and VEM mRNA
106 from targeted cells could transfer these mRNA to other cells and amplify the protein
107 output of the cell population. To enable this, we engineered MEFI by inserting MS2
108 aptamers into the 3′UTR of VEM mRNA, enabling self-packaging into VLPs upon
109 translation (Figure 1I).

110 To determine the efficiency of MEFI to re-package and export cargo mRNA,
111 mCherry alone, mCherry plus VEM, and mCherry plus MEFI plasmids were
112 transfected into 293T cell, respectively. After 36 hours, the supernatants were filtered
113 and added to the RAW264.7 cells. Then, the mixed culture media was replaced with
114 fresh media 6 hours later to remove residue VLPs, and 24 hours later, the supernatants
115 were collected for qPCR assay. The results indicated that MEFI enriched almost 10^8-
116 fold of mCherry mRNA compared to mCherry alone. In contrast, VEM enriched
117 mCherry mRNA by ~2-fold compared to mCherry alone. In parallel, a similar result
118 was obteined when assessing the VSVg mRNA, suggesting MEFI protein can
119 efficiently export itself mRNA (Figure 1J).

120 To determine whether external MEFI can export endogenous MS2-tagged mRNA
121 from targeted cells, we transfected the NLuc-MS2 plasmid alone, which is convenient
122 for quantitative detection, into RAW264.7 cells. After 24 hours, the indicated
123 supernatants were added, and NLuc in the cells was detected by chemiluminescence
124 following an additional 24-hour infection period. We observed that the addition of VEM
125 supernatant did not increase the expression of NLuc, while MEFI increased the
126 expression of NLuc by approximately 10-fold. Subsequently, the cell supernatants from
127 the previous step were added to fresh RAW264.7 cells. The luminescence assay
128 revealed that the supernatant produced by VEM exhibited a slight increase, whereas
129 MEFI achieved an approximate 100-fold enhancement in NLuc expression, thereby

130 demonstrating intercelluar ferrying of cargo mRNA (Figure 1K). We then showed that
131 MS2 is indispensable for cargo mRNA intercellular transfer, as MEFI does not enhance
132 the expression of NLuc mRNA without MS2 in cells by transient plasimd transfection
133 and supernatant infection (Figure 1L). Next, in order to assess the efficiency of multiple
134 rounds, or iterative, delivery of mRNA by MEFI, mouse embryo fibroblasts (MEFs)
135 were used to infect with the supernatant of previous round (Figure S1D). Although each
136 round of Nluc expression is attenuated over the previous one, we could still detect the
137 expression of Nluc after seven rounds of MEFI propagation (Figure 1M). Collectively,
138 these results provide compelling evidence that MEFI can facilitate the iterative delivery
139 of cargo mRNA through recursive VLP assembly and intercellular transfer.

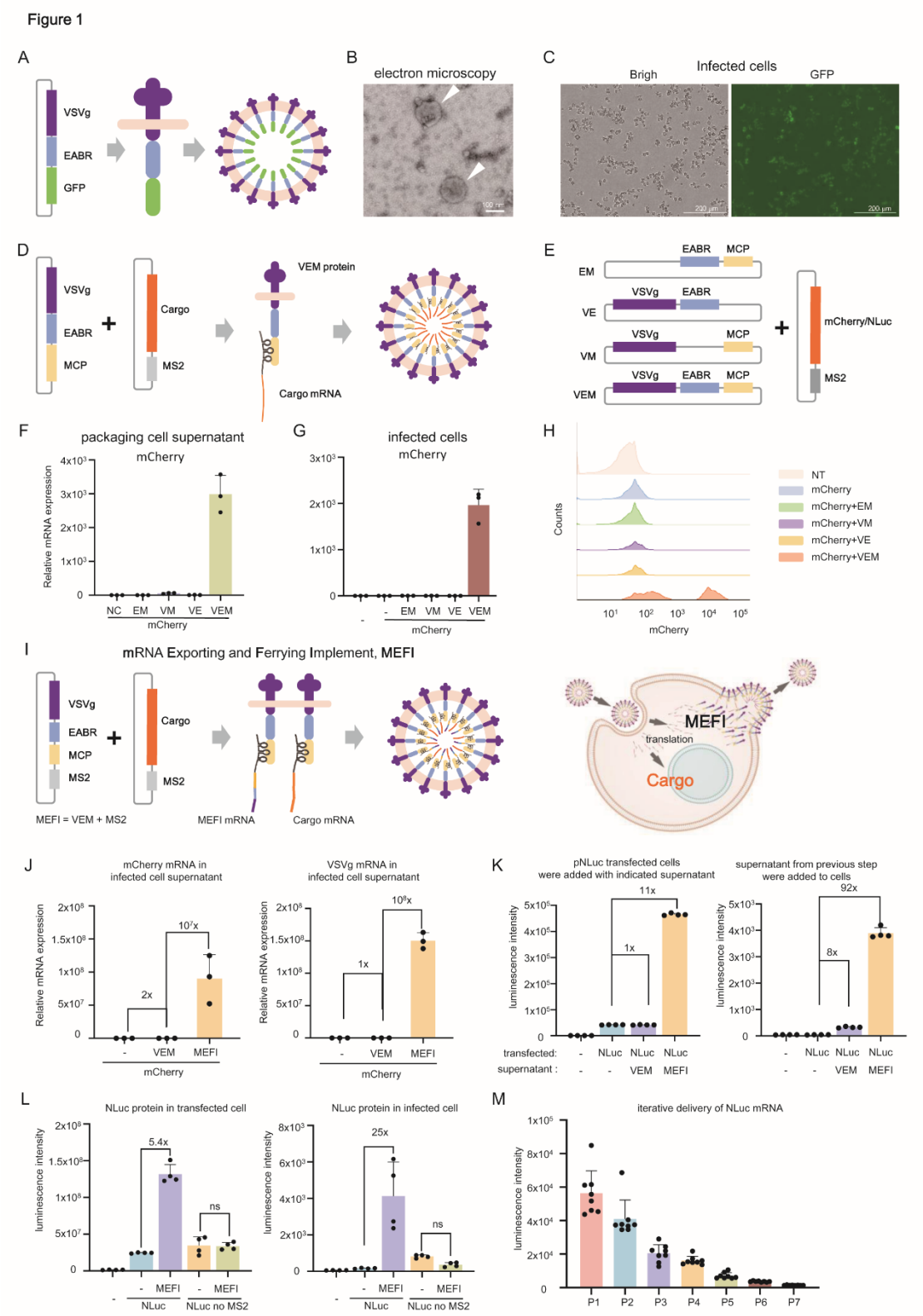

Figure 1. MEFI encodes fusion protein packages mRNA into self-propagating VLPs, enabling continuous cell-to-cell transfer

(A) VSVg-EABR-GFP fusion protein facilitates the assembly of VLP (schematic).

144 (B) VSVg-EABR-GFP VLP purified from transfected 293T cell culture supernatants
145 by ultracentrifugation on a 20% sucrose cushion. Particles were visualized using uranyl
146 acetate negative staining and imaged using a transmission electron microscope. Scale
147 bars, 100 nm. Magnification, ×180,000.
148 (C) RAW264.7 cells were infected with VLPs from B for 24 h before fluorescence
149 images were taken.
150 (D) The schematic diagram shows VSVg-EABR-MCP fusion protein facilitates the
151 assembly of VLP, which packages cargo mRNA.
152 (E) The schematic diagram illustrates the composition of VSVg-EABR-MCP and its
153 truncations.
154 (F) The relative quantity of mCherry-MS2 mRNA in the supernatants of 293T cells
155 transfected for 36 h with the indicated plasmids by qPCR assay. Each dot represents
156 one technical replicate.
157 (G) The relative quantity of mCherry-MS2 mRNA in RAW264.7 cells infected with the
158 supernatants indicated in (F) for 24 hours by qPCR assay. Each dot represents one
159 technical replicate.
160 (H) Flow cytometry conducted on cells from (G).
161 (I) The schematic diagram shows MEFI facilitates the assembly of VLP, which
162 packages both cargo and itself mRNA, enabling reproduction in infected cell.
163 (J) The indicated plasmids were transfected into 293T cell. After 36 hours, the
164 supernatants were filtered and added to RAW264.7 cells. Then, the mixed culture media
165 was replaced with fresh media 6 hour later to remove residue VLPs, and 24 hr later, the
166 supernatants were collected for qPCR assay.
167 (K) RAW264.7 cells were transfected with pNLuc plasmids, and 293T cells were
168 transfected with either VEM or MEFI plasmids. After 24 hours, the supernatants from
169 the transfected 293T cells were added to the RAW264.7 cells. The expression of NLuc
170 in these cells was then detected using chemiluminescence after an additional 24 hours
171 (left). Concurrently, the supernatants from the RAW264.7 cells were transferred to a
172 fresh batch of RAW264.7 cells. 24 hours later, the expression of NLuc in these cells

173 was also measured using chemiluminescence (right).

174 (L) The indicated plasmids were transfected into 293T cells. After 36 hours, the NLuc
175 expression was measured using chemiluminescence (left). Concurrently, the
176 supernatants were transferred to RAW264.7 cells. Another 24 hours later, the
177 expression of NLuc in these cells was measured using chemiluminescence (right).

178 (M) 293T cells were co-transfected with NLuc-MS2 and MEFI plasmids, 36 hours later,
179 the supernatant were filtered and added to MEFs. After 6 hours, the media was replaced
180 with fresh one. Another 18 hours later, the expression of NLuc was measured, and the
181 supernatants were transferred to a fresh batch of MEFs. This round was conducted 7
182 times as described in Fig S1D.

183 The optimized MEFI system enhances cargo expression and crosses biological 184 barriers

185 Now that MEFI is capable of conducting cargo mRNA transfer from cell to cell, we
186 next determine whether MEFI can enhance the production of total cargo protein. First,
187 GFP-MS2 alone, GFP-MS2 plus VEM, and GFP-MS2 plus MEFI plasmids were
188 transfected into 293T cell, respectively. The flow cytometry assay indicated that co-
189 transfection with VEM increased the rate of GFP^+ cells and the mean fluorescence
190 intensity (MFI) of the total cell population compared to that of GFP alone. Furthermore,
191 MEFI significantly increased the rate of GFP^+ cells and the MFI of the total cell
192 population. Additionally, we found that neither VEM nor MEFI decreased the mean
193 fluorescence intensity (MFI) of the GFP^+ cells, suggesting that the exporting of GFP
194 mRNA did not reduce GFP protein production in individual cells (Figure S2 A).
195 Moreover, the single MEFI-cargo fused mRNA did not transfer as effectively as the
196 pattern of separated MEFI and cargo mRNA (Figure S2 B-C). Then, we performed
197 codon and secondary structure optimization of MEFI mRNA using the LinearDesign
198 tool[39,40]: Codon Adaption Index of MEFI increased from (CAI) 0.75 to 0.93, minimal
199 free energy (MFE) decreased from -856.30 to -1478.40 kcal/mol (Figure S2 D). We
200 found that the optimized MEFI had an ~2 folds improved capacity to enhance Nluc
201 expression (Figure S2 E). Thereafter, MEFI indicates the optimized version.

202 Next, we optimized the mass ratio of cargo to MEFI by transfecting a fixed quantity of
203 the NLuc plasmid (pNLuc) with varying quantities of the MEFI plasmid (pMEFI).We
204 observed a 5-fold increase in NLuc expression at a initial ratio of 1:0.5 compared to
205 that at 1:0 (NLuc alone). MEFI exhibited maximal potency at a 1:2 ratio, with a 25-fold
206 enhancement in expression compared to NLuc alone (Figure 2A). When the total
207 plasmid quantity was fixed, the highest NLuc expression occured at a ratio of 1:2 again,
208 with a 8-fold increase in expression compared to NLuc alone (Figure 2B). We also
209 observed that while achieving the same level of NLuc expression, MEFI reduced total
210 plasmid amount to at least one-tenth of that required for pNLuc alone (Figure 2C).
211 Thereafter, unless otherwise specified, we adopt a MEFI: cargo ratio of 2:1.

212 Effective systemic delivery of plasmid DNA presents a significant challenge[41]. We
213 then evaluated MEFI's efficacy in promoting plasmid DNA expression by means of in
214 vivo and ex vivo luminescence. The indicated plasmids were encapsulated in a
215 commercial cationic lipids. After 24 hours of intravenous injection, mice in the pNLuc
216 alone group exhibited nearly undetectable expression of NLuc, whereas in the presence
217 of MEFI, NLuc expression was ~ 360-fold compared to that of the pNLuc alone (Figure
218 2D). A strong expression of NLuc persisted at least 72 hours facilitated by MEFI, and
219 then the mice were sacrificed for organs ex vivo imaging. Weak NLuc expression was
220 detected only in the lungs and spleens of mice treated with pNLuc alone, whereas the
221 presence of MEFI resulted in substantially higher NLuc expression in most major
222 organs compared to that of pNLuc alone: 501-fold higher in the lung, 147-fold higher
223 in the liver, 85-fold higher in the spleen, 53-fold higher in the brain (Figure 2E), 27-
224 fold higher in the kidneys, 50-fold higher in the heart, 35-fold higher in the pancreas,
225 and 142-fold higher in the inguinal lymph nodes (Figure S2F). Importantly, the obvious
226 expression of NLuc in the brain indicates that MEFI could transfer cargo mRNA across
227 the blood-brain barrier (Figure 2E).

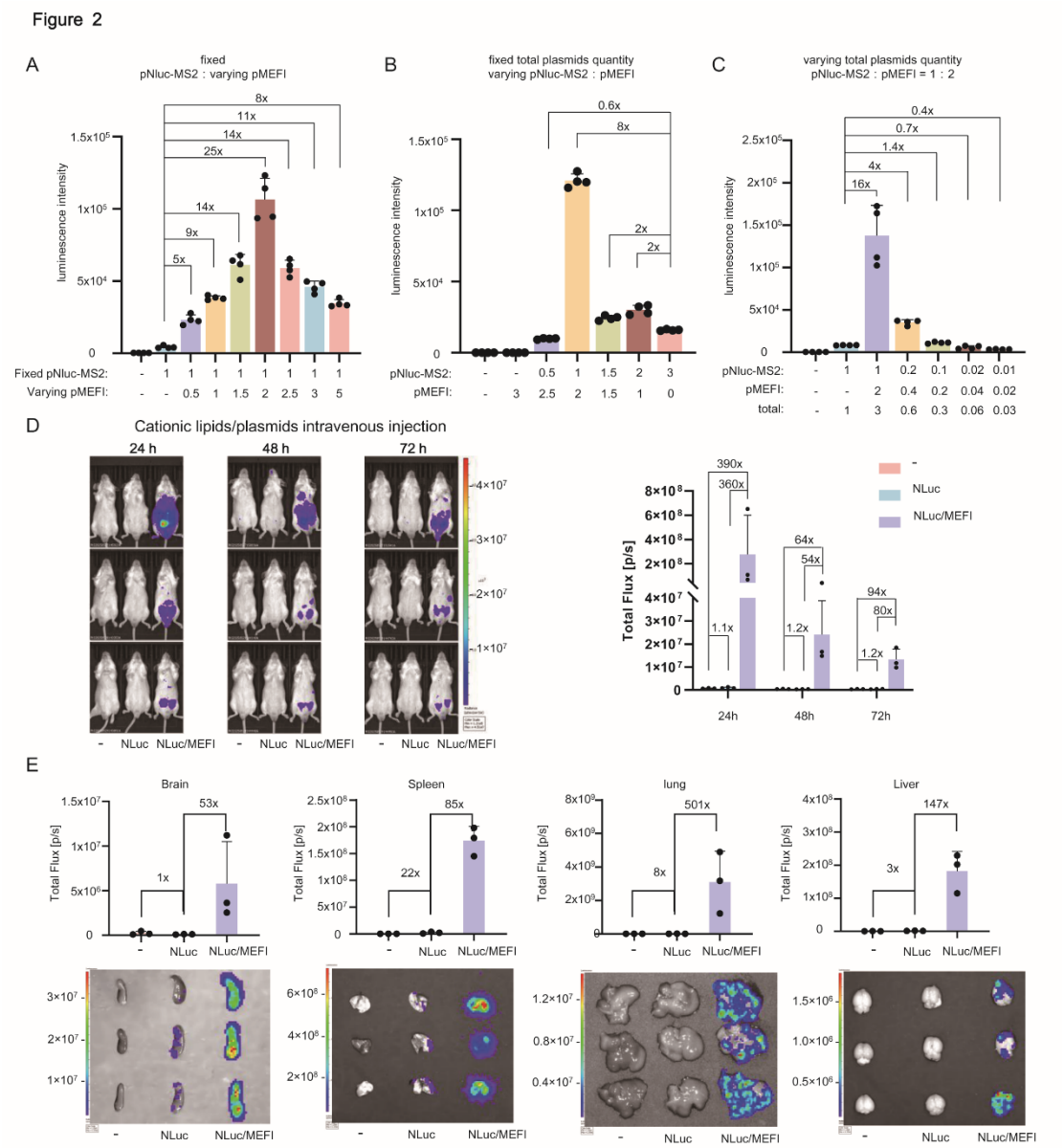

Figure 2. The optimized MEFI system enhances cargo expression *in vitro and in vivo*

(A-C) The indicated plasmids were transfected into RAW264.7 cells. After 36 hours, the NLuc expression was measured using chemiluminescence.

(D) Whole-body bioluminescent imaging of mice after intravenous injection with indicated plasmids (pNLuc, 5 μg/mice; pMEFI, 10 μg/mice) encapsulated within cationic lipids. (n =3)

(E) Ex vivo organ bioluminescence from mice of (D) 72 hours after injection.

MEFI enables robust and dureble expression of naked plasmids and interorgan

238 **cargo transfer *in vivo***

239 Intramuscular injection of naked plasmids is the one of most convenient methods of
240 gene delivery, however, the effect is poor due to the low level of cargo protein
241 expression[42,43]. Next, we attempt to evaluate whether MEFI can enhance cargo
242 expression through intramuscular injection of naked plasmids. For the relative
243 uniformity of the comparison, the same mouse was injected with pNLuc plus pGFP into
244 the left caudal thigh muscle, while pNLuc plus pMEFI were injected into the right
245 caudal thigh muscle. Indeed, we did not detect obvious NLuc expression from the left
246 side, but a robust NLuc expression was observed on the right side up to two months
247 post-injection. Moreover, a second administration still evoked significant and durable
248 NLuc expression, suggesting that MEFI and its protein did not elicit an obvious
249 adaptive immune response (Figure 3A-B). We then examined the ability of MEFI to
250 deliver therapeutic naked pDNA cargo via intramuscular injection. 28 days post-
251 administration, we detected therapeutic levels of human erythropoietin (hEPO) in the
252 serum of mice injected with phEPO/pMEFI, whereas no detectable hEPO was present
253 in the absence of MEFI (Figure 3C).

254 To further confirm whether MEFI can mediate cargo mRNA transfer *in vivo*, we utilized
255 genetically engineered ZsGreen/tdTomato conversion reporter mice (CAG-LoxP-
256 ZsGreen-Stop-LoxP-tdTomato) containing a LoxP-flanked ZsGreen-STOP cassette
257 that initially expresses ZsGreen but prevents the expression of the tdTomato protein.
258 Once the ZsGreen-STOP cassette is deleted by Cre, ZsGreen expression is turned off,
259 and tdTomato fluorescence is turned on, allowing for the detection of Cre-mediated
260 gene-edited cells. Seven days following the intramuscular injection of the MS2-tagged
261 Cre plasmid and pMEFI, tdTomato fluorescence was readily detected in some organs
262 through ex vivo imaging (Figure 3D). Additionally, tdTomato-positive cells were easily
263 observed using confocal imaging of tissue sections (Figures 3E, S3B). Specifically,
264 tdTomato-positive cells were emerging in the brain, demonstrating that MEFI facilitates
265 Cre mRNA crossing the blood-brain barrier (Figure 3E). These findings suggest that
266 MEFI can facilitate interorgan cargo mRNA transfer in mice.

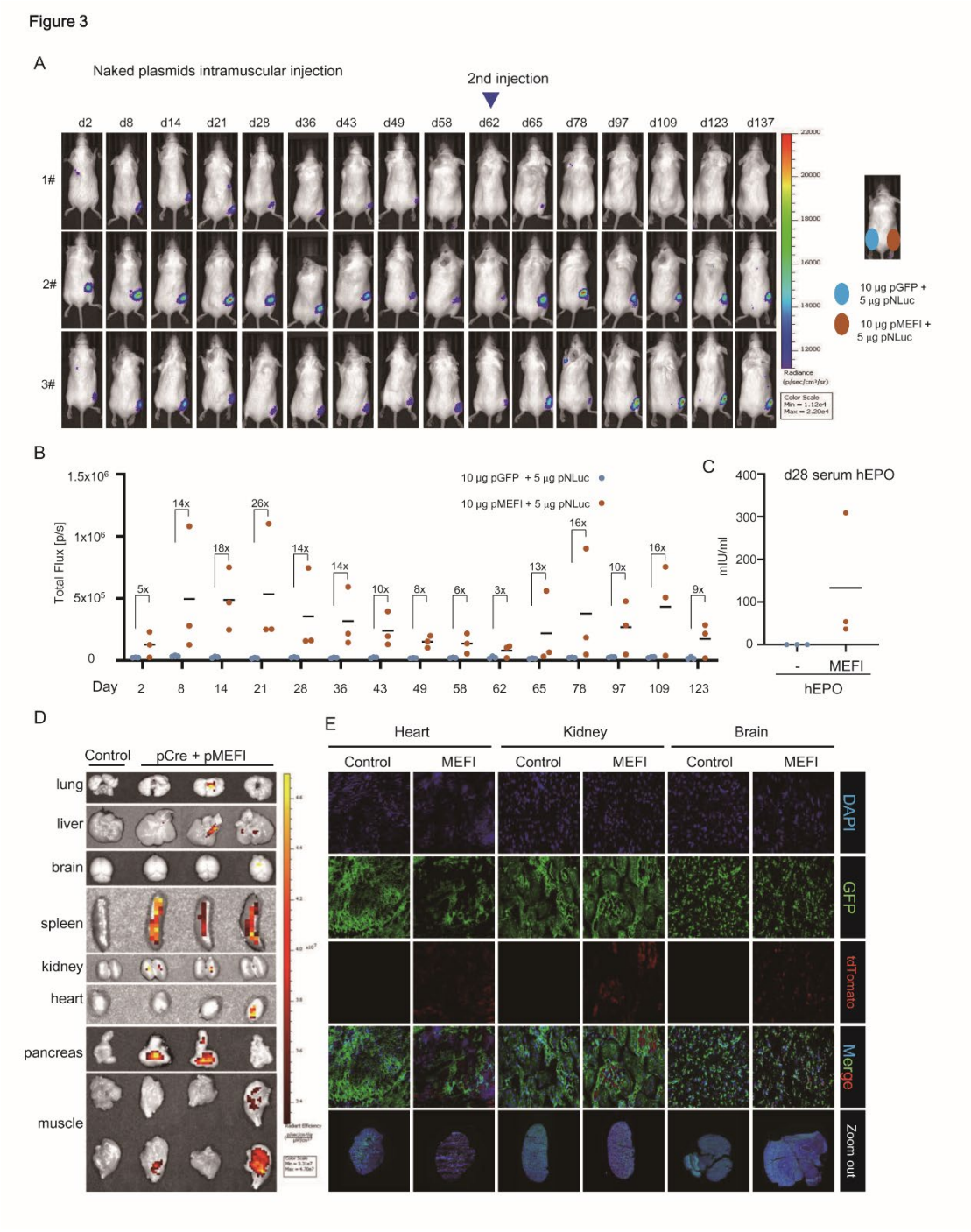

Figure 3. MEFI enables robust and dureble expression of naked plasmids and interorgan cargo transfer in vivo

(A) Whole-body bioluminescent imaging of mice after intramuscular injection with indicated naked plasmids. The same mouse was injected with pNLuc plus pGFP into the left caudal thigh muscle, while pNLuc plus pMEFI were injected into the right caudal thigh muscle. (n =3)

(B) Quantification of bioluminescent signal from (A).

275 (C) Serum hEPO concentrations in mice which were intramuscular injected with
276 indicated naked plasmids 28 days ago, n = 3 biologically independent mice per group.
277 (D) Ex vivo organ tdTomato fluorescence from mice that were intramuscularly
278 injected with the indicated naked plasmids 7 days prior (n=3).
279 (E) Confocal imaging of tissue sections of mice from (D).

280 **Cell type-specific cytotoxicity conducted by scFv-MEFI**

281 Next, we aim to modify MEFI for cell-specific delivery. Reports indicate that by fusing
282 a single-chain variable fragment (scFv) between the secretion signal and
283 transmembrane domain of VSVg, its antigen targeting tropism can be achieved[44-46].
284 Inspired by this, we constructed MEFI variants targeting CD19 and tyrosinase-related
285 protein 1 (TYRP1, a melanoma surface antigen) by replacing the extracellular domain
286 of VSVg with the corresponding anti-CD19 or anti-TYRP1 scFv, respectively (Figure
287 4A). Then, we used NLuc as cargo to verify the specific targeting of scFv-MEFI. The
288 chemiluminescence assay revealed that in the presence of MEFI or anti-CD19 scFv-
289 MEFI, the expression of NLuc in Naml6 cells ($CD19^+$), were almost equal. However,
290 the anti-CD19 scFv-MEFI was inefficient in transferring NLuc mRNA to K562 cells
291 ($CD19^-$) compared to native MEFI (Figure 4B). A similar result was obtained in the
292 items of anti-TYRP1 MEFI in $TYRP1^+$ B16 and $TYRP1^-$ GL261 cells (Figure 4C)

293 Diphtheria toxin A chain (DTA), a widely used inducer of cell death[47], was selected
294 as the cargo to test the cell type specific killing of scFv-MEFI. Twenty-four hours after
295 adding the indicated transiently co-transfected supernatant, the ATP assay demonstrated
296 the cell viability of Nalm6 cells were both decreased in the present of MEFI and anti-
297 CD19 scFv-MEFI. However, compared with that of anti-CD19 MEFI, only the MEFI
298 DTA-treated K562 cells were obviously killed (Figure 4D). A similar result was
299 obtained in the items of anti-TYRP1 MEFI with $TYRP1^+$ B16 and $TYRP1^-$ GL261 cells,
300 confirming its cell-type cytotoxicity (Figure 4E).

301 Compared to traditional small-molecule proteolysis targeting chimeras
302 (PROTACs), biological PROTACs expand the range of targeted proteins with a more
303 flexible E3 ligase selection[48-50]. However, the challenges associated with specific

intracellular delivery limit their application. We thus utilized a bioPROTAC, targeting the oncology-related protein Proliferating Cell Nuclear Antigen (PCNA), as a cargo to assess the specific delivery of scFv-MEFI. The ATP assay revealed a more significant reduction in the viability of Nalm6 cells treated with the supernatant from anti-CD19-MEFI/aPCNA-PROTAC compared to those treated with the supernatant from MEFI/aPCNA-PROTAC. However, the cell viability of K562 cells was more decreased in the presence of MEFI-PROTAC than with anti-CD19 scFv-MEFI-PROTAC (Figure S4A). A similar result was obtained for the anti-TYRP1 MEFI with both TYRP1^{+} B16 and TYRP1^{-} GL261 cells (Figure S4B). These results demonstrate that MEFI can be modified for cell-specific targeting to deliver diverse therapeutic cargoes.

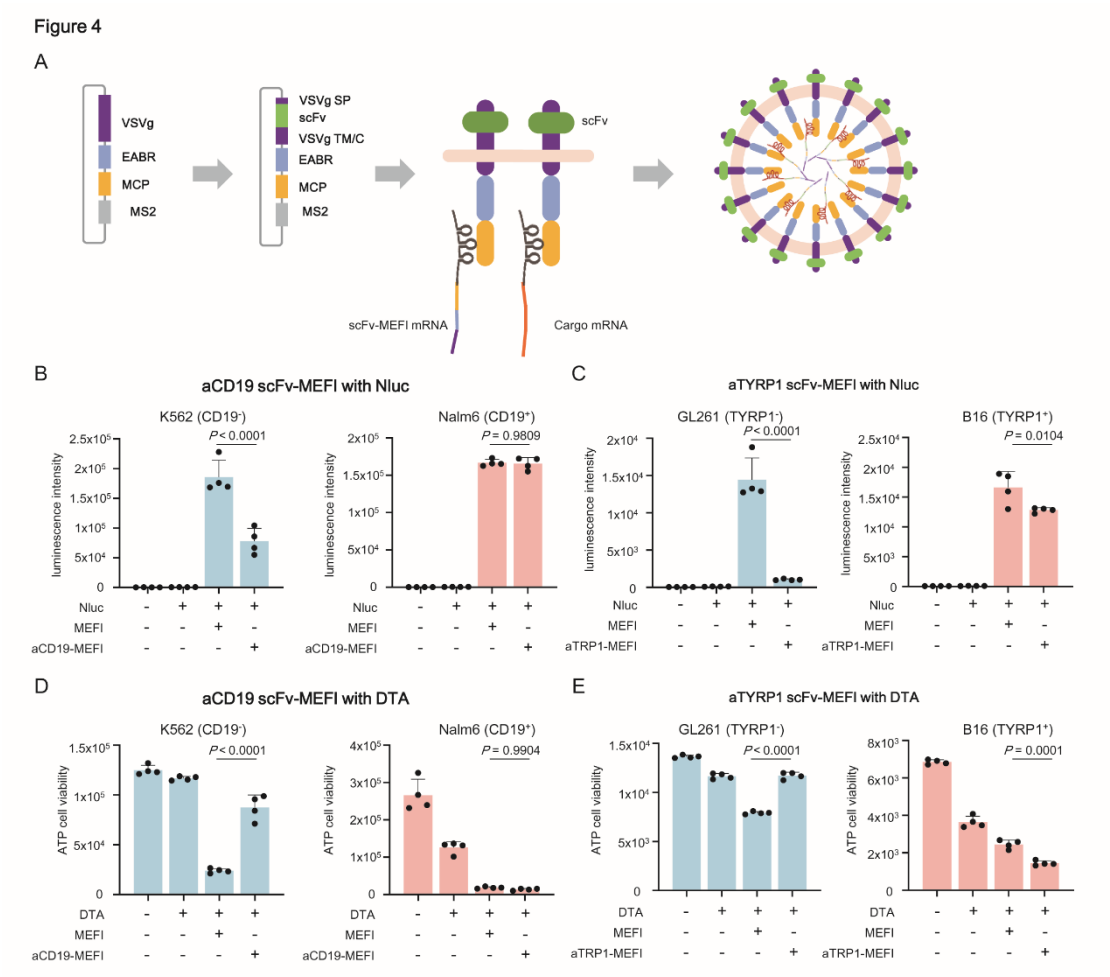

Figure 4. Cell type-specific cytotoxicity conducted by scFv-MEFI

(A) The schematic diagram shows scFv-MEFI facilitates the assembly of VLP, which packages both cargo and itself mRNA.

318 (B-C) The indicated plasmids were transfected into 293T cell. After 36 hours, the
319 supernatants were filtered and added to indicated cells. 24 hours later, the NLuc
320 expression was measured using chemiluminescence.
321 (D-E) The indicated plasmids were transfected into 293T cell. After 36 hours, the
322 supernatants were filtered and added to indicated cells. 24 hours later, the cell viablity
323 was measured by ATP assay.
324

Discussion

The development of the mRNA Exporting and Ferrying Implement (MEFI) represents a paradigm shift in mRNA therapeutics, as it enables iterative, cell-to-cell transfer of cargo mRNA. Unlike conventional mRNA delivery systems where mRNA functions transiently within a single cell, MEFI harnesses a self-replicating VLP system to amplify cargo expression across cellular barriers, significantly enhancing therapeutic potency and durability.

MEFI's core innovation lies in its ability to package both cargo mRNA and its own mRNA into fusogenic VLPs, enabling continuous propagation from primary to secondary target cells. This "multiple-use" effect addresses a fundamental limitation of short-lived expression of current mRNA therapies by extending cargo availability across cell populations. MEFI enhances low-efficiency delivery methods (e.g., naked plasmid intramuscular injection) by orders of magnitude, potentially revolutionizing DNA vaccine strategies. The sustained protein production by naked plasmid intramuscular injection for two months underscore its potential for long-term treatments, such as protein replacement therapies. The ability to cross the blood-brain barrier further expands applications to neurological disorders. By replacing VSVg's extracellular domain with specific scFvs (anti-CD19/anti-TYRP1), MEFI achieves cell-type-specific cargo delivery. This modular targeting system enabled selective cytotoxicity in antigen-positive cells using lethal cargoes (DTA) or bioPROTACs, while sparing off-target cells. Such precision could mitigate systemic toxicity in oncology and expand the scope of biologics delivery, including previously undruggable intracellular targets.

Unlike conventional eVLPs requiring multiple viral components, MEFI's single VEM fusion protein simplifies production and reduces immunogenicity. Its capsid-independent assembly bypasses packaging constraints of lentiviral systems. While delivered mRNA to primary cells, MEFI enables secondary spread, amplifying effects in poorly accessible tissues (e.g., brain, solid tumors). Although adaptive immunity against MEFI was minimal, long-term studies must assess anti-fusogen responses.

Engineering hypoimmunogenic variants (e.g., humanized fusogens) could mitigate risks. Attenuation over transfer rounds may reflect mRNA degradation or translational silencing. Incorporating RNA-stabilizing elements (e.g., UTR optimization, nucleotide modifications or circular mRNA) could enhance persistence. While scFv-MEFI showed promising specificity, in vivo validation in complex microenvironments is needed. Alternative targeting moieties (e.g., de novo designed binders[52]) may improve affinity. Expanding beyond MS2-MCP systems (e.g., using L7Ae-kink-turn[53]) could enable alternative applications.

MEFI establishes a modular, extensible platform that transforms mRNA from a transient payload into a self-propagating therapeutic agent. Its capacity for iterative delivery, systemic amplification, and cell-specific targeting positions it as a platform technology for next-generation biologics. Future work will focus on optimizing safety profiles, extending cargo diversity (e.g., base editors, transcription factors, large transgenes), and advancing toward clinical translation in oncology, genetic disorders, and regenerative medicine in animal models, organoids and patients.

RESOURCE AVAILABILITY

Lead contact

Further information and requests for resources and reagents should be directed to and will be fulfilled by the lead contact, Xiushan Yin, (xiushanyin@me.com)

DATA AVAILABILITY STATEMENT

The data that support the findings of this study are available from the corresponding author upon reasonable request.

ACKNOWLEDGMENTS

This work was supported by Roc Rock Biotechnology (Suzhou) Co., Ltd. The research project was funded partially by the the National Natural Science Foundation of China (32371490) and Beijing Municipal Natural Science Foundation (5252022) to L.Z. Additional support was provided by the 2023 National Center for Biotechnology Innovation in Cellular Therapy Technology Research Project (2023XB0010) to X.Y.

AUTHOR CONTRIBUTIONS

L.Z. and X.S.Y. conceptualized this work. L.Z., X.S.Y., Y.G., H.L., Y.X., Y.L., Y.F.L., S.L., X.J.S., X.B.F., J.H.L., Q.Y.Z., and X.S.Y. developed the methodology. Y.G., L.Z., X.S.Y., H.L., Y.X., Y.L., Y.F.L., S.L., X.J.S., X.B.F., J.H.L. and Q.Y.Z. carried out the investigation. L.Z., Y.G., H.L., Y.X., Y.L., Y.F.L., S.L., X.J.S., X.B.F. and J.H.L. created visual representations. L.Z., Y.G. and X.S.Y. wrote the initial draft and L.Z., Y.G., X.S.Y., H.L., Y.X. and X.B.F. reviewed and edited the manuscript. L.Z. and X.S.Y. were responsible for funding acquisition and project administration.

DECLARATION OF INTERESTS

X.S.Y. is inventor of the described technology and have filed patent applications through Roc Rock Biotechnology (Suzhou) Co., Ltd. All other authors declare no competing interests.

ORCID

Luo Zhang https://orcid.org/ 0000-0002-7688-5955

Xiushan Yin https://orcid.org/ 0000-0001-8124-7387

References

1. McNamara, J.O., 2nd, and Giangrande, P.H. (2024). Toward the full potential of mRNA therapeutics. Molecular therapy : the journal of the American Society of Gene Therapy *32*, 1600-1601. 10.1016/j.ymthe.2024.05.012.
2. Parhiz, H., Atochina-Vasserman, E.N., and Weissman, D. (2024). mRNA-based therapeutics: looking beyond COVID-19 vaccines. Lancet *403*, 1192-1204. 10.1016/S0140-6736(23)02444-3.
3. Liu, C., Shi, Q., Huang, X., Koo, S., Kong, N., and Tao, W. (2023). mRNA-based cancer therapeutics. Nature reviews. Cancer *23*, 526-543. 10.1038/s41568-023-00586-2.
4. Popovitz, J., Sharma, R., Hoshyar, R., Soo Kim, B., Murthy, N., and Lee, K. (2023). Gene editing therapeutics based on mRNA delivery. Advanced drug delivery reviews *200*, 115026. 10.1016/j.addr.2023.115026.
5. Muik, A., Lui, B.G., Wallisch, A.K., Bacher, M., Muhl, J., Reinholz, J., Ozhelvaci, O., Beckmann, N., Guimil Garcia, R.C., Poran, A., et al. (2022). Neutralization of SARS-CoV-2 Omicron by BNT162b2 mRNA vaccine-elicited human sera. Science *375*, 678-680. 10.1126/science.abn7591.
6. Nemet, I., Kliker, L., Lustig, Y., Zuckerman, N., Erster, O., Cohen, C., Kreiss, Y., Alroy-Preis, S., Regev-Yochay, G., Mendelson, E., and Mandelboim, M. (2022). Third BNT162b2 Vaccination Neutralization of SARS-CoV-2 Omicron Infection. The New England journal of medicine *386*, 492-494. 10.1056/NEJMc2119358.
7. Lu, C., Li, Y., Cummings, J.R., and Banskota, S. (2025). Delivery of genome editors with engineered virus-like particles. Methods in enzymology *712*, 475-516. 10.1016/bs.mie.2025.01.007.
8. Ikwuagwu, B., and Tullman-Ercek, D. (2022). Virus-like particles for drug delivery: a review of methods and applications. Current opinion in biotechnology *78*, 102785. 10.1016/j.copbio.2022.102785.
9. Hill, B.D., Zak, A., Khera, E., and Wen, F. (2018). Engineering Virus-like Particles for Antigen and Drug Delivery. Current protein & peptide science *19*, 112-127. 10.2174/1389203718666161122113041.
10. Rohovie, M.J., Nagasawa, M., and Swartz, J.R. (2017). Virus-like particles: Next-generation nanoparticles for targeted therapeutic delivery. Bioengineering & translational medicine *2*, 43-57. 10.1002/btm2.10049.
11. Hamann, M.V., Stanke, N., Mullers, E., Stirnnagel, K., Hutter, S., Artegiani, B., Bragado Alonso, S., Calegari, F., and Lindemann, D. (2014). Efficient transient genetic manipulation in vitro and in vivo by prototype foamy virus-mediated nonviral RNA transfer. Molecular therapy : the journal of the American Society of Gene Therapy *22*, 1460-1471. 10.1038/mt.2014.82.
12. Xu, Y.F., Zhang, Y.Q., Xu, X.M., and Song, G.X. (2006). Papillomavirus virus-like particles as vehicles for the delivery of epitopes or genes. Archives of virology *151*, 2133-2148. 10.1007/s00705-006-0798-8.
13. Horns, F., Martinez, J.A., Fan, C., Haque, M., Linton, J.M., Tobin, V., Santat, L., Maggiolo, A.O., Bjorkman, P.J., Lois, C., and Elowitz, M.B. (2023). Engineering RNA export for measurement and manipulation of living cells. Cell *186*, 3642-3658 e3632. 10.1016/j.cell.2023.06.013.

448 14. Brown, D.W., Wee, P., Bhandari, P., Bukhari, A., Grin, L., Vega, H., Hejazi, M., Sosnowski,
449 D., Ablack, J., Clancy, E.K., et al. (2024). Safe and effective in vivo delivery of DNA and
450 RNA using proteolipid vehicles. Cell *187*, 5357-5375 e5324. 10.1016/j.cell.2024.07.023.
451 15. Banskota, S., Raguram, A., Suh, S., Du, S.W., Davis, J.R., Choi, E.H., Wang, X., Nielsen,
452 S.C., Newby, G.A., Randolph, P.B., et al. (2022). Engineered virus-like particles for efficient
453 in vivo delivery of therapeutic proteins. Cell *185*, 250-265 e216. 10.1016/j.cell.2021.12.021.
454 16. Ling, S., Yang, S., Hu, X., Yin, D., Dai, Y., Qian, X., Wang, D., Pan, X., Hong, J., Sun, X., et
455 al. (2021). Lentiviral delivery of co-packaged Cas9 mRNA and a Vegfa-targeting guide RNA
456 prevents wet age-related macular degeneration in mice. Nature biomedical engineering *5*, 144-
457 156. 10.1038/s41551-020-00656-y.
458 17. An, M., Raguram, A., Du, S.W., Banskota, S., Davis, J.R., Newby, G.A., Chen, P.Z.,
459 Palczewski, K., and Liu, D.R. (2024). Engineered virus-like particles for transient delivery of
460 prime editor ribonucleoprotein complexes in vivo. Nature biotechnology *42*, 1526-1537.
461 10.1038/s41587-023-02078-y.
462 18. Segel, M., Lash, B., Song, J., Ladha, A., Liu, C.C., Jin, X., Mekhedov, S.L., Macrae, R.K.,
463 Koonin, E.V., and Zhang, F. (2021). Mammalian retrovirus-like protein PEG10 packages its
464 own mRNA and can be pseudotyped for mRNA delivery. Science *373*, 882-889.
465 10.1126/science.abg6155.
466 19. Lu, B., Javidi-Parsijani, P., Makani, V., Mehraein-Ghomi, F., Sarhan, W.M., Sun, D., Yoo,
467 K.W., Atala, Z.P., Lyu, P., and Atala, A. (2019). Delivering SaCas9 mRNA by lentivirus-like
468 bionanoparticles for transient expression and efficient genome editing. Nucleic acids research
469 *47*, e44. 10.1093/nar/gkz093.
470 20. Sun, Y., Sun, Y., Zhao, R., and Gao, K. (2016). Intracellular delivery of messenger RNA by
471 recombinant PP7 virus-like particles carrying low molecular weight protamine. BMC
472 biotechnology *16*, 46. 10.1186/s12896-016-0274-9.
473 21. Mohsen, M.O., Gomes, A.C., Vogel, M., and Bachmann, M.F. (2018). Interaction of Viral
474 Capsid-Derived Virus-Like Particles (VLPs) with the Innate Immune System. Vaccines *6*.
475 10.3390/vaccines6030037.
476 22. Mangeot, P.E., Dollet, S., Girard, M., Ciancia, C., Joly, S., Peschanski, M., and Lotteau, V.
477 (2011). Protein transfer into human cells by VSV-G-induced nanovesicles. Molecular therapy :
478 the journal of the American Society of Gene Therapy *19*, 1656-1666. 10.1038/mt.2011.138.
479 23. Garrus, J.E., von Schwedler, U.K., Pornillos, O.W., Morham, S.G., Zavitz, K.H., Wang, H.E.,
480 Wettstein, D.A., Stray, K.M., Cote, M., Rich, R.L., et al. (2001). Tsg101 and the vacuolar
481 protein sorting pathway are essential for HIV-1 budding. Cell *107*, 55-65. 10.1016/s0092-
482 8674(01)00506-2.
483 24. Fujii, K., Munshi, U.M., Ablan, S.D., Demirov, D.G., Soheilian, F., Nagashima, K., Stephen,
484 A.G., Fisher, R.J., and Freed, E.O. (2009). Functional role of Alix in HIV-1 replication.
485 Virology *391*, 284-292. 10.1016/j.virol.2009.06.016.
486 25. Fisher, R.D., Chung, H.Y., Zhai, Q., Robinson, H., Sundquist, W.I., and Hill, C.P. (2007).
487 Structural and biochemical studies of ALIX/AIP1 and its role in retrovirus budding. Cell *128*,
488 841-852. 10.1016/j.cell.2007.01.035.
489 26. Matsuo, H., Chevallier, J., Mayran, N., Le Blanc, I., Ferguson, C., Faure, J., Blanc, N.S.,
490 Matile, S., Dubochet, J., Sadoul, R., et al. (2004). Role of LBPA and Alix in multivesicular
491 liposome formation and endosome organization. Science *303*, 531-534.

492 10.1126/science.1092425.
493 27. Strack, B., Calistri, A., Craig, S., Popova, E., and Gottlinger, H.G. (2003). AIP1/ALIX is a
494 binding partner for HIV-1 p6 and EIAV p9 functioning in virus budding. Cell *114*, 689-699.
495 10.1016/s0092-8674(03)00653-6.
496 28. Votteler, J., and Sundquist, W.I. (2013). Virus budding and the ESCRT pathway. Cell host &
497 microbe *14*, 232-241. 10.1016/j.chom.2013.08.012.
498 29. Pincetic, A., Medina, G., Carter, C., and Leis, J. (2008). Avian sarcoma virus and human
499 immunodeficiency virus, type 1 use different subsets of ESCRT proteins to facilitate the
500 budding process. The Journal of biological chemistry *283*, 29822-29830.
501 10.1074/jbc.M804157200.
502 30. Lee, H.H., Elia, N., Ghirlando, R., Lippincott-Schwartz, J., and Hurley, J.H. (2008). Midbody
503 targeting of the ESCRT machinery by a noncanonical coiled coil in CEP55. Science *322*, 576-
504 580. 10.1126/science.1162042.
505 31. Zhao, W.M., Seki, A., and Fang, G. (2006). Cep55, a microtubule-bundling protein, associates
506 with centralspindlin to control the midbody integrity and cell abscission during cytokinesis.
507 Molecular biology of the cell *17*, 3881-3896. 10.1091/mbc.e06-01-0015.
508 32. Fabbro, M., Zhou, B.B., Takahashi, M., Sarcevic, B., Lal, P., Graham, M.E., Gabrielli, B.G.,
509 Robinson, P.J., Nigg, E.A., Ono, Y., and Khanna, K.K. (2005). Cdk1/Erk2- and Plk1-
510 dependent phosphorylation of a centrosome protein, Cep55, is required for its recruitment to
511 midbody and cytokinesis. Developmental cell *9*, 477-488. 10.1016/j.devcel.2005.09.003.
512 33. Hoffmann, M.A.G., Yang, Z., Huey-Tubman, K.E., Cohen, A.A., Gnanapragasam, P.N.P.,
513 Nakatomi, L.M., Storm, K.N., Moon, W.J., Lin, P.J.C., West, A.P., Jr., and Bjorkman, P.J.
514 (2023). ESCRT recruitment to SARS-CoV-2 spike induces virus-like particles that improve
515 mRNA vaccines. Cell *186*, 2380-2391 e2389. 10.1016/j.cell.2023.04.024.
516 34. Fu, Y., and Li, J. (2016). A novel delivery platform based on Bacteriophage MS2 virus-like
517 particles. Virus research *211*, 9-16. 10.1016/j.virusres.2015.08.022.
518 35. Ashley, C.E., Carnes, E.C., Phillips, G.K., Durfee, P.N., Buley, M.D., Lino, C.A., Padilla,
519 D.P., Phillips, B., Carter, M.B., Willman, C.L., et al. (2011). Cell-specific delivery of diverse
520 cargos by bacteriophage MS2 virus-like particles. ACS nano *5*, 5729-5745.
521 10.1021/nn201397z.
522 36. Pan, Y., Zhang, Y., Jia, T., Zhang, K., Li, J., and Wang, L. (2012). Development of a
523 microRNA delivery system based on bacteriophage MS2 virus-like particles. The FEBS
524 journal *279*, 1198-1208. 10.1111/j.1742-4658.2012.08512.x.
525 37. Nikolic, J., Belot, L., Raux, H., Legrand, P., Gaudin, Y., and A, A.A. (2018). Structural basis
526 for the recognition of LDL-receptor family members by VSV glycoprotein. Nature
527 communications *9*, 1029. 10.1038/s41467-018-03432-4.
528 38. Finkelshtein, D., Werman, A., Novick, D., Barak, S., and Rubinstein, M. (2013). LDL receptor
529 and its family members serve as the cellular receptors for vesicular stomatitis virus.
530 Proceedings of the National Academy of Sciences of the United States of America *110*, 7306-
531 7311. 10.1073/pnas.1214441110.
532 39. Leppek, K., Byeon, G.W., Kladwang, W., Wayment-Steele, H.K., Kerr, C.H., Xu, A.F., Kim,
533 D.S., Topkar, V.V., Choe, C., Rothschild, D., et al. (2022). Combinatorial optimization of
534 mRNA structure, stability, and translation for RNA-based therapeutics. Nature
535 communications *13*, 1536. 10.1038/s41467-022-28776-w.

40. Zhang, H., Zhang, L., Lin, A., Xu, C., Li, Z., Liu, K., Liu, B., Ma, X., Zhao, F., Jiang, H., et al. (2023). Algorithm for optimized mRNA design improves stability and immunogenicity. Nature *621*, 396-403. 10.1038/s41586-023-06127-z.
41. Patel, M.N., Tiwari, S., Wang, Y., O'Neill, S., Wu, J., Omo-Lamai, S., Espy, C., Chase, L.S., Majumder, A., Hoffman, E., et al. (2025). Safer non-viral DNA delivery using lipid nanoparticles loaded with endogenous anti-inflammatory lipids. Nature biotechnology. 10.1038/s41587-025-02556-5.
42. Wang, C., and Yuan, F. (2024). A comprehensive comparison of DNA and RNA vaccines. Advanced drug delivery reviews *210*, 115340. 10.1016/j.addr.2024.115340.
43. Singh, A.K., Goel, K., and Dhanawat, M. (2025). Plasmid DNA and mRNA delivery: Approaches and challenges. Advances in immunology *165*, 63-87. 10.1016/bs.ai.2024.12.001.
44. Strebinger, D., Frangieh, C.J., Friedrich, M.J., Faure, G., Macrae, R.K., and Zhang, F. (2023). Cell type-specific delivery by modular envelope design. Nature communications *14*, 5141. 10.1038/s41467-023-40788-8.
45. Yu, B., Shi, Q., Belk, J.A., Yost, K.E., Parker, K.R., Li, R., Liu, B.B., Huang, H., Lingwood, D., Greenleaf, W.J., et al. (2022). Engineered cell entry links receptor biology with single-cell genomics. Cell *185*, 4904-4920 e4922. 10.1016/j.cell.2022.11.016.
46. Dobson, C.S., Reich, A.N., Gaglione, S., Smith, B.E., Kim, E.J., Dong, J., Ronsard, L., Okonkwo, V., Lingwood, D., Dougan, M., et al. (2022). Antigen identification and high-throughput interaction mapping by reprogramming viral entry. Nature methods *19*, 449-460. 10.1038/s41592-022-01436-z.
47. Thorburn, J., Frankel, A.E., and Thorburn, A. (2003). Apoptosis by leukemia cell-targeted diphtheria toxin occurs via receptor-independent activation of Fas-associated death domain protein. Clinical cancer research : an official journal of the American Association for Cancer Research *9*, 861-865.
48. Fletcher, A., Clift, D., de Vries, E., Martinez Cuesta, S., Malcolm, T., Meghini, F., Chaerkady, R., Wang, J., Chiang, A., Weng, S.H.S., et al. (2023). A TRIM21-based bioPROTAC highlights the therapeutic benefit of HuR degradation. Nature communications *14*, 7093. 10.1038/s41467-023-42546-2.
49. Chan, A., Haley, R.M., Najar, M.A., Gonzalez-Martinez, D., Bugaj, L.J., Burslem, G.M., Mitchell, M.J., and Tsourkas, A. (2024). Lipid-mediated intracellular delivery of recombinant bioPROTACs for the rapid degradation of undruggable proteins. Nature communications *15*, 5808. 10.1038/s41467-024-50235-x.
50. Lim, S., Khoo, R., Peh, K.M., Teo, J., Chang, S.C., Ng, S., Beilhartz, G.L., Melnyk, R.A., Johannes, C.W., Brown, C.J., et al. (2020). bioPROTACs as versatile modulators of intracellular therapeutic targets including proliferating cell nuclear antigen (PCNA). Proceedings of the National Academy of Sciences of the United States of America *117*, 5791-5800. 10.1073/pnas.1920251117.
51. Li, B., Jiang, A.Y., Raji, I., Atyeo, C., Raimondo, T.M., Gordon, A.G.R., Rhym, L.H., Samad, T., MacIsaac, C., Witten, J., et al. (2025). Enhancing the immunogenicity of lipid-nanoparticle mRNA vaccines by adjuvanting the ionizable lipid and the mRNA. Nature biomedical engineering *9*, 167-184. 10.1038/s41551-023-01082-6.
52. Vazquez Torres, S., Leung, P.J.Y., Venkatesh, P., Lutz, I.D., Hink, F., Huynh, H.H., Becker, J., Yeh, A.H., Juergens, D., Bennett, N.R., et al. (2024). De novo design of high-affinity binders

of bioactive helical peptides. Nature *626*, 435-442. 10.1038/s41586-023-06953-1.

53. Saito, H., Kobayashi, T., Hara, T., Fujita, Y., Hayashi, K., Furushima, R., and Inoue, T. (2010). Synthetic translational regulation by an L7Ae-kink-turn RNP switch. Nature chemical biology *6*, 71-78. 10.1038/nchembio.273.

586 **KEY RESOURCES TABLE**

REAGENT or RESOURCE	SOURECE	IDENTIFIER
Chemicals, peptides, and recombinant proteins		
Dulbecco's Modified Eagle Medium	Gibco	21063029
Roswell Park Memorial Institute (RPMI) 1640 Medium with GlutaMAX supplement	Corning	10-040-CVRC
Fetal bovine serum	EXCELL	FND500
Penicillin-Streptomycin-Glutamine	Thermo Fisher Scientific	15140-122
Trypsin-EDTA Solution	TBD	TE2004Y
PBS	TBD	PB2004Y
jetPRIME Transfection Reagent	Polyplus	101000046
in vivo-jetPEI	Polyplus	101000030
L-glutamine	Thermo Fisher Scientific	25030-081
DMSO	Sango	A600163-0250
Absolute ethyl alcohol	Sango	A500737-0500
Phosphotungstic acid	Rhawn	R128447
Uranyl acetate	TED PELLA	19481
Furimazine	Macklin	F882901
OCT compound	SAKURA	BE6140
Critical commercial assays		
QIAamp Viral RNA Mini Kit		
Transcriptor reverse transcriptase	Vazyme	R312-02
Eastep Super Total RNA Extraction Kit	Promega	LS1040
TBGreen™ Premix Ex Taq™ II	Takara	632200

CellTiter-Glo® Luminescent Cell Viability Assay	Promega	G7570
Human EPO ELISA kit	Boster	EK0332
Experimental models: Cell lines		
293T	ATCC	CRL-3216
RAW264.7	ATCC	SC-6005
GL261	ATCC	HB-12317
K562	ATCC	CRL-3344
B16	ATCC	CRL-6475
Nalm-6	ATCC	CRL-3273
other		
6-well plates	Thermo Fisher Scientific	140675
10 cm culture dish	Corning	430167
12-well plates	Nest Scientific	712002
100 μm mesh Steriflip cell strainer	Corning	352360
0.45 mm filter membrane	Pall Corporation	4614
15 ml centrifuge tube	Nest Scientific	601002
50 ml centrifuge tube	Corning	339652
Amicon Ultra-15 Centrifugal Filter	Millipore	UFC910024
Copper mesh	EMCN. Co	N/A
Oligonucleotides		
mCherry qPCR forward primer	GeneUnivesal	CACGAGTTCGAGATCGAGGG
mCherry qPCR reverse primer	GeneUnivesal	CAAGTAGTCGGGGATGTCGG
Nluc qPCR forward primer	GeneUnivesal	GGATTGTCCTGAGCGGTGAA
Nluc qPCR reverse primer	GeneUnivesal	CATCCACAGGGTACACCACC
VSVG qPCR forward primer	GeneUnivesal	AGATGCCCAAGTCCCACAAG
VSVG qPCR reverse primer	GeneUnivesal	CTCGATGCTCTCCTTGCACT
GAPDH qPCR forward primer	GeneUnivesal	ACTCCACTCACGGCAAATTC

GAPDH qPCR reverse primer	GeneUnivesal	TCTCCATGGTGGTGAAGACA
Recombinant DNA		
pMD-EABR-MS2-GFP	This paper	N/A
pCMV-EABR-MCP	This paper	N/A
pCMV-VSVG-EABR	This paper	N/A
pCMV-VSVG-MCP	This paper	N/A
pCMV-VSVG-EABR-MCP	This paper	N/A
pCMV-Nluc-MS2	This paper	N/A
pCMV-Nluc	This paper	N/A
pCMV-mCherry-MS2	This paper	N/A
pCMV-GFP-MS2	This paper	N/A
pCMV-hEPO-MS2	This paper	N/A
pCMV-cre-MS2	This paper	N/A
pCMV-DTA-MS2	This paper	N/A
pCMV-ProTac-MS2	This paper	N/A
pCMV-GmRbdC3d-MS2	This paper	N/A
pAd-MEFI	This paper	N/A
pAd-MEFI-P2A-Nluc	This paper	N/A
pAd-mCMV-EGFP	This paper	N/A
pAd-aCD19-MEFI	This paper	N/A
pAd-aTYRP1-MEFI	This paper	N/A
pAd-covSP-MEFI	This paper	N/A

EXPERIMENTAL MODEL AND STUDY PARTICIPANT DETAILS

Cell lines

HEK293T and GL261 cells were cultured in Dulbecco's modified Eagle's medium (DMEM, Gibco) supplemented with 10% heat-inactivated fetal bovine serum (FBS, EXCELL) and 1% penicillin-streptomycin (Gibco) at 37°C and 5% CO_2. RAW264.7, K562, Nalm-6, and B16 cells are cultured in Roswell Park Memorial Institute (RPMI)

594 1640 Medium supplemented with 10% FBS and 1% penicillin-streptomycin.

595

596 **Plasmid construction**

597 Constructs used in this study are listed in the key resources table. Some constructs were
598 generated by standard cloning procedures, in which inserts and linearized backbones
599 were generated by polymerase chain reaction (PCR) or restriction digest. The remaining
600 constructs were designed by the authors and synthesized by GeneUnivesal.

601

602 **Mouse studies**

603 Animals were group-housed in IVCs under SPF conditions, with constant temperature
604 and humidity with lighting on a fixed light/dark cycle (12-hours/12-hours). 5 – 7 weeks
605 old homozygous mouse littermates were randomly assigned to experimental groups.
606 No mice were involved in previous procedures.

607 In vivo studies were done using adult, 8–10-week-old, male BALB/c (Charles River
608 Laboratories, Beijing, China) (Figure 2D). Intravenous injection occurred via the lateral
609 tail vein with 100 μL of the test agent. Furimazine solution was injected
610 intraperitoneally at the specified time point into both acquisition and analysis of optical
611 images.

612 In vivo studies were done using adult, 8–10-week-old, female BALB/c (Charles River
613 Laboratories, BeiJing, China) (Figure 3A). Intramuscular injection occurred in the
614 lateral muscle group of the thigh with 80 μL of the test agent.

615 In vivo studies were done using adult, 8–12-week-old, male B6-G/R (RocRock
616 Laboratories, Shenyang, China) (Figure 3D). Intramuscular injection occurred in the
617 lateral muscle group of the thigh with 80 μL of the test agent.

618

619 **METHODS DETAILS**

620 **VLP production**

621 VLPs in our paper were produced by transient transfection of HEK293T cells.
622 HEK293T cells were seeded in 6-well plates at a density of 5 x 10^5 cells per well. After

623 24h, cells were transfected using the jetPRIME transfection reagent according to the
624 manufacturer's protocols. The reagent volume to DNA mass ratio(V/m) was 1:2 (fill-
625 up with JetOPTIMUS Buffer, 10 min incubation at room temperature for complex
626 formation). The detailed plasmid stoichiometries of the different systems are shown in
627 this paper. The media was changed after 6 hours, and VLP supernatant was harvested
628 at 36 hr and centrifuged for 5 min at 500 g to remove cell debris. The clarified VLP-
629 containing supernatant was filtered through a 0.45-mm filter. For VLPs that were used
630 in cell culture, unless otherwise stated, the filtered supernatant was concentrated 100-
631 fold using Amicon Ultra-15 Centrifugal Filter. Ultracentrifugation was performed at
632 135,000 g for 2 h (4°C) using an SW 40Ti rotor in an Optima XPN-80 Ultracentrifuge
633 (Beckman Coulter). Following ultracentrifugation, VLP pellets were resuspended in
634 cold PBS. Samples were aliquoted and stored at -20°C.
635 For making specific receptor targeting and integrating VLPs, VSV-G mutant was used
636 instead.
637
638 **Lentiviral infection and viral incubation assay**
639 To evaluate VLPs, 20 μL concentrated EABR-VLP was added into RAW264.7 cells in
640 12 well plate. 2 days later, GFP signal was measured by flow cytometry. To define the
641 roles of VSVg, EABR, and MCP in mRNA packaging and delivery, 40 μL concentrated
642 VLPs were added into RAW264.7 cells in 6 well plate. Upon 2 days incubation, cells
643 were subjected to flow cytometry to quantify mCherry+ cells.
644
645 **Negative-stain transmission electron microscopy**
646 VLPs were centrifuged for 5 min at 500 g to remove debris and then the clarified
647 supernatant were ultracentrifuged for 2 hrs at 135,000 g. A drop of 10 μL of sample was
648 applied to a carbon coated grid that had been glow discharged for 1 min in air, and the
649 grids were immediately negatively stained using 2% phosphotungstic acid for 60 s.
650 Grids were examined in a H-7800 operated at 80-120 kV. Images were taken using
651 HITACHI Transmission Electron Microscope.

652

653 **Bioluminescence quantification**

654 NLuc signal was read on-plate 48 hours post-transfection. Measurements were taken
655 on a BioTek synergy H1 plate reads with 1 s acquisition time right after the addition of
656 Furimazine (Macklin) for NLuc.

657

658 **Flow cytometry**

659 48 h post-incubation by VLPs, cells were gently detached in a suitable volume of
660 accutase, pelleted (500 g, 5 min), and resuspended in PBS. Analysis was performed on
661 the BD FACS machine. Data were analyzed with FlowJo. The main population of the
662 cells was gated according to their FSC-A and SSC-A. About the single cells were gated
663 using FSC-A and FSC-H.

664

665 **Reverse transcription and quantitative PCR**

666 We used an RT-qPCR assay to measure the abundance of specific RNA molecules in
667 VLP or cellular RNA. The VLP RNA was extracted from 10 mL of supernatant using
668 the Viral RNA Mini kit according to manufacturer's instructions. The cellular RNA was
669 extracted from cells using the Eastep Super Total RNA Extraction Kit according to
670 manufacturer's instructions. RNA was then reverse transcribed using Transcriptor
671 reverse transcriptase mix at 42 °C for 15 mins, and 95 °C for 3 mins. Quantitative
672 polymerase chain reaction (qPCR) was performed on the CFX96 Touch system (Biorad)
673 using SYBR Green Supermix with reverse transcription product as input, final
674 concentration of 400 nM per primer, and thermal cycling profile consisting of 95 °C for
675 30 seconds, followed by 40 cycles of 95 °C for 10 seconds and 60 °C for 30 seconds.
676 Primer sequences are listed in key resources table. Negative controls consisting of
677 supernatant from HEK293T cells subjected to mock transfections without DNA.

678

679 **ELISAs**

680 Serum EPO levels were quantified using the BOSTER Human EPO Assay kit following

681 the manufacturer's instructions. First of all, plates are coated with biotinylated capture
682 antibody prior to sample and standard administration. Samples and standards are
683 incubated on plate for 90 mins at 37 °C, following which detection antibody is added
684 for 1 hour. Avidin-peroxidase complex was added to the plate for 30 mins incubation,
685 and then it was analyzed with the BioTek synergy H1.
686
687 **Cell viability assays**
688 Cell viability was quantified using a Promega CellTiter-Glo luminescent cell viability
689 kit. $5x10^4$ cells (forB16, Nalm-6, GL261 and K562) were seeded in 100 μL of media
690 per well. The cells were allowed to adhere for 24 h before treatment with VLPs. After
691 48 h of VLP incubation, 100 μL of CellTiter-Glo reagent was added to each well in the
692 dark. Cells were incubated for 10 min at room temperature and the 100 μL of solution
693 was transferred into black 96-well flat bottom plates, and the luminescence was
694 measured on a BioTek synergy H1 plate reads with 1 s acquisition time.
695
696 **Histofluorescence staining**
697 Tissues were fixed in 4% paraformaldehyde (PFA) for 24 h, dehydrated in 30% sucrose
698 solution. Frozen sections were preserved in OCT compound, frozen, sectioned at 3 μm,
699 and stored at -80 °C. Prior to staining, all samples were rinsed with ddH2O. The
700 sections were then incubated 5 minutes at room temperature with 5 μg/mL DAPI away
701 from light, then washed with ddH2O. Images were captured using a confocal
702 microscopy system (LSM 700, Zeiss, Jena, Germany). Image analysis was performed
703 in ImageJ.
704